



PEDOT:PSS:sulfonium salt composite hole injection layers for efficient organic light emitting diodes

Apostolis Verykios^{a,b}, Giorgos Pistolis^a, Lambros Bizas^a, Charalambos Tselios^c, Dimitris Tsikritzis^c, Stella Kennou^c, Christos L. Chochos^d, Dionysis E. Mouzakis^e, Panagiotis N. Skandamis^f, Abd Rashid bin Mohd Yusoff^g, Leonidas C. Palilis^b, Panagiotis Argitis^a, Maria Vasilopoulou^{a,**}, Anastasia Soultati^{a,*}

^a Institute of Nanoscience and Nanotechnology, National Center for Scientific Research Demokritos, Agia Paraskevi, 15341, Athens, Greece

^b Department of Physics, University of Patras, 26504, Patras, Greece

^c Surface Science Laboratory, Department of Chemical Engineering, University of Patras, 26504, Patras, Greece

^d Institute of Chemical Biology, National Hellenic Research Foundation, 48 Vassileos Constantinou Avenue, Athens, 11635, Greece

^e Hellenic Army Academy, Department of Military Services, Greece

^f Agricultural University of Athens, Department of Food Science and Human Nutrition, Laboratory of Food Quality Control and Hygiene, Iera Odos 75, 11855, Athens, Greece

^g Department of Chemical Engineering, Pohang University of Science and Technology (POSTECH), Pohang, Gyeongbuk 37673, Republic of Korea

ARTICLE INFO

Keywords:

Triphenylsulfonium salt
PEDOT:PSS
Hole injection layer
Organic light emitting diodes
Interface engineering

ABSTRACT

In this work, we propose a simple and effective approach to modify the optoelectronic properties of the commonly used poly(3,4-ethylenedioxythiophene):poly(styrene sulfonate) (PEDOT:PSS) and consequently to improve hole injection and transport in organic light emitting diodes (OLEDs) using emissive layers based on a fluorescence copolymer. In particular, two triphenylsulfonium (TPS) salts that consist of the same TPS cation and two different counter anions, in particular, hexafluoroantimonate (SbF₆) and trifluoromethane sulfonate (Triflate) were added in the PEDOT:PSS solution in various concentrations and the composite films were fully characterized for surface and optoelectronic properties and subsequently we employed as hole injection layers (HILs) in OLEDs. It is demonstrated that both, the counter anion and the concentration of TPS-salts in the PEDOT:PSS matrix play significant role in the optoelectronic properties of the composite and thus in the device performance. Although all TPS-salt modified PEDOT:PSS films exhibited higher work function (W_F) values relative to the undoped one thus resulting in more efficient hole injection than pristine PEDOT:PSS, the PEDOT:PSS:TPS-Triflate with the lower concentration (10:1 v/v) showed the highest luminous (LE) and power efficiency (PE) values of 27.04 cd A⁻¹ and 6.26 lm W⁻¹, respectively. This extraordinary performance was ascribed to a significant increase in the conductivity of the composite film combined with the formation of an interface exciplex between the TPS-Triflate (acceptor) and the emissive copolymer (donor). This interfacial electroplex strongly confines the generated excitons and prevents their diffusion towards aluminum cathode which acts as exciton quencher.

1. Introduction

Since the first publication on organic electroluminescent devices by Tang and Van Slyke in 1987 [1], organic light-emitting diodes (OLEDs) have emerged as a mature technology, and nowadays OLED displays and lighting panels are constantly gaining significant market penetration.

However, they still attract extensive research interest aiming to further improvements in the device performance such as high brightness and low operation voltage combined with high operational stability and inexpensive fabrication [2,3]. Solution-processing is a promising approach to low-cost OLEDs fabrication using easily implemented materials with facile deposition methods.

* Corresponding author.

** Corresponding author.

E-mail address: asoultati@inn.demokritos.gr (A. Soultati).

<https://doi.org/10.1016/j.orgel.2021.106155>

Received 24 November 2020; Received in revised form 15 February 2021; Accepted 14 March 2021

Available online 1 April 2021

1566-1199/© 2021 Elsevier B.V. All rights reserved.

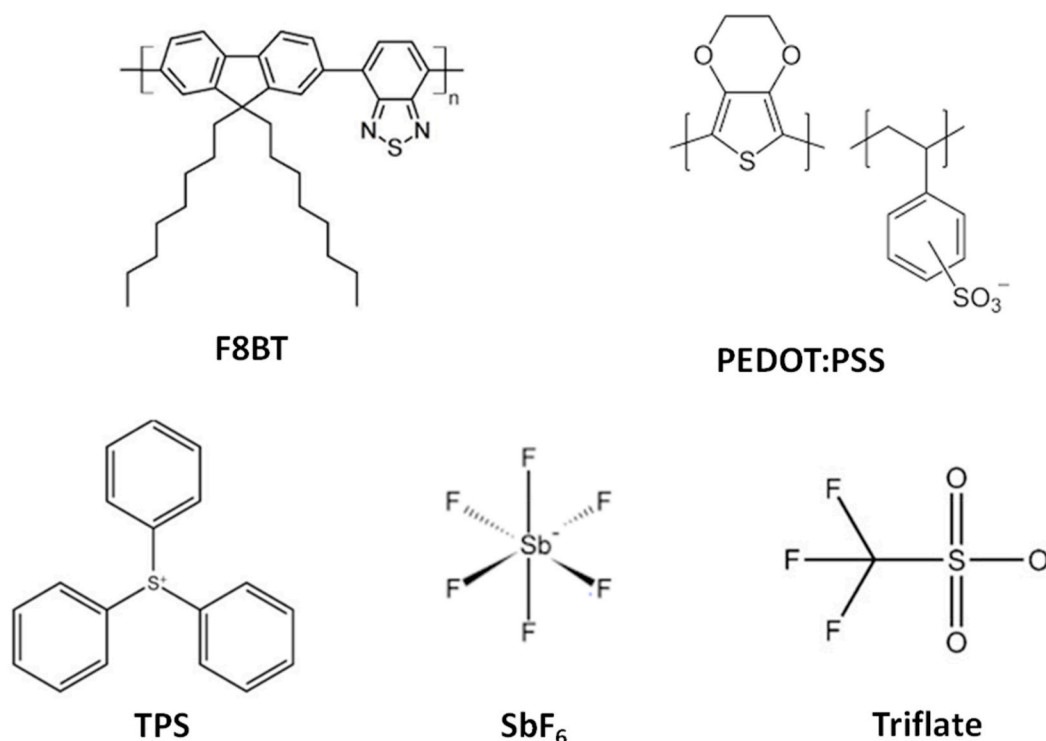


Fig. 1. Chemical structures of the materials used in this study. Copolymer F8BT and PEDOT:PSS was the emissive and HIL of the fabricated OLEDs, respectively, while TPS-salts consisting of TPS cation and/or SbF₆ and triflate counterions used as PEDOT:PSS dopants and also employed as HILs.

The structure of an OLED is based on the multi-layered architecture, where the emissive layer (EML) and the charge carrier transport materials are sandwiched between two electrodes. The role of the hole and electron transport materials (HTM/ETM) is crucial as they facilitate balanced charge carrier injection/transport within the emissive layer and thus improve the exciton generation rate and device efficiency [4, 5]. These charge injection and transport materials have to meet several requirements in order to reduce charge injection barrier and facilitate carrier transport from the electrode toward the EML, such as good carrier mobility, high-transparency in the visible region when inserted at the light extraction interface, well-matched energy levels with the organic semiconductor used in the emissive layer and smooth film formation [6–10].

Hole injection layers (HILs), in particular, such as p-type organic semiconductors (OSCs) and high W_F transition metal oxides (TMOs) have been effectively incorporated in OLEDs to modify the optoelectronic properties of the widely used indium-tin oxide (ITO) transparent anode [11–21]. Among them, PEDOT:PSS, which is a p-type OSC with high hole mobility, is the most commonly used HIL in OLEDs with the conventional architecture (that is, anode/HIL/EML/EIL/cathode, where EIL refers to the electron injection layer whereas the bottom anode usually consists of ITO) due to its high W_F value of 5.2 eV [22]. It is also highly-transparent in the visible region, thermally stable and forms a smooth film via aqueous solution-processing [23,24]. Despite these excellent properties, PEDOT:PSS suffers from low conductivity and is extremely hydroscopic which might be detrimental for the device stability [25].

One strategy to improve the conductivity of PEDOT:PSS is the addition of dopants such as organic small molecules [26], nanoparticles [27], ionic liquids [28] and carbon nanotubes [29,30]. Highly-conductive PEDOT:PSS films are also reported through post-treatment with H₂SO₄, hexafluoroacetone or methanol solvents [31]. Moreover, the addition of TMOs in the PEDOT:PSS solution improves the conductivity of the HILs used in highly-efficient OLEDs. Recently, Yadav et al. [32], studied the vanadium oxide (V₂O₅) doping

effect of PEDOT:PSS HIL on the device performance demonstrating lower turn-on voltage and higher efficiency for the V₂O₅-doped PEDOT:PSS-based OLED compared with the device with the pristine PEDOT:PSS HIL. Also, Jeong et al. [33], proposed an effective molecular scale control strategy to improve the properties of PEDOT:PSS through the implementation of effective co-additives composed of alkylammonium halides, polar solvent, and perfluorinated ionomers. With their method, the authors managed to simultaneously increase the conductivity and W_F of the polymer anode while maintaining its exciton blocking capability, thus demonstrating highly efficient perovskite LEDs. More recently, Zeng et al. [34], reported that the addition of dopamine hydrochloride into PEDOT:PSS enhanced its conductivity along with the W_F leading to improved performance of organic solar cells.

Triphenylsulfonium (TPS) salts are a widely studied class of ionic compounds, commonly used as photoacid generators (PAGs) in lithographic processing and photoresist technology [35–37]. The incorporation of TPS salts in polyfluorene-based OLEDs has been previously investigated by our group [38]. It was demonstrated that the addition of TPS salts in the polyfluorene-based EML significantly enhanced the device performance, ascribed to the TPS anions movement towards the ITO anode and their accumulation therein that lead to the formation of a local electric field that improved the hole injection efficiency. Consequently, the devices with the optimum TPS salt concentration showed high luminous efficiency along with low turn-on and operating voltages. In a further work [39], we studied the effect of the counter anion on the optoelectronic properties of TPS-based OLEDs using four TPS salts with the same cation and different counter anions. Interestingly, the size and the nature of the anion played a critical role in the charge injection and transport, as well as, the emission profile of the OLED based on TPS salts. The photochemical tuning of the emission color of a single polymeric layer defining the three primary colors was also demonstrated via the addition of a TPS salt in the emissive layer of the OLED [40]. Moreover, improved device characteristics were exhibited attributed to the facile charge injection and transport in the TPS salt-based OLED.

In the current work, motivated by the attractive properties of TPS

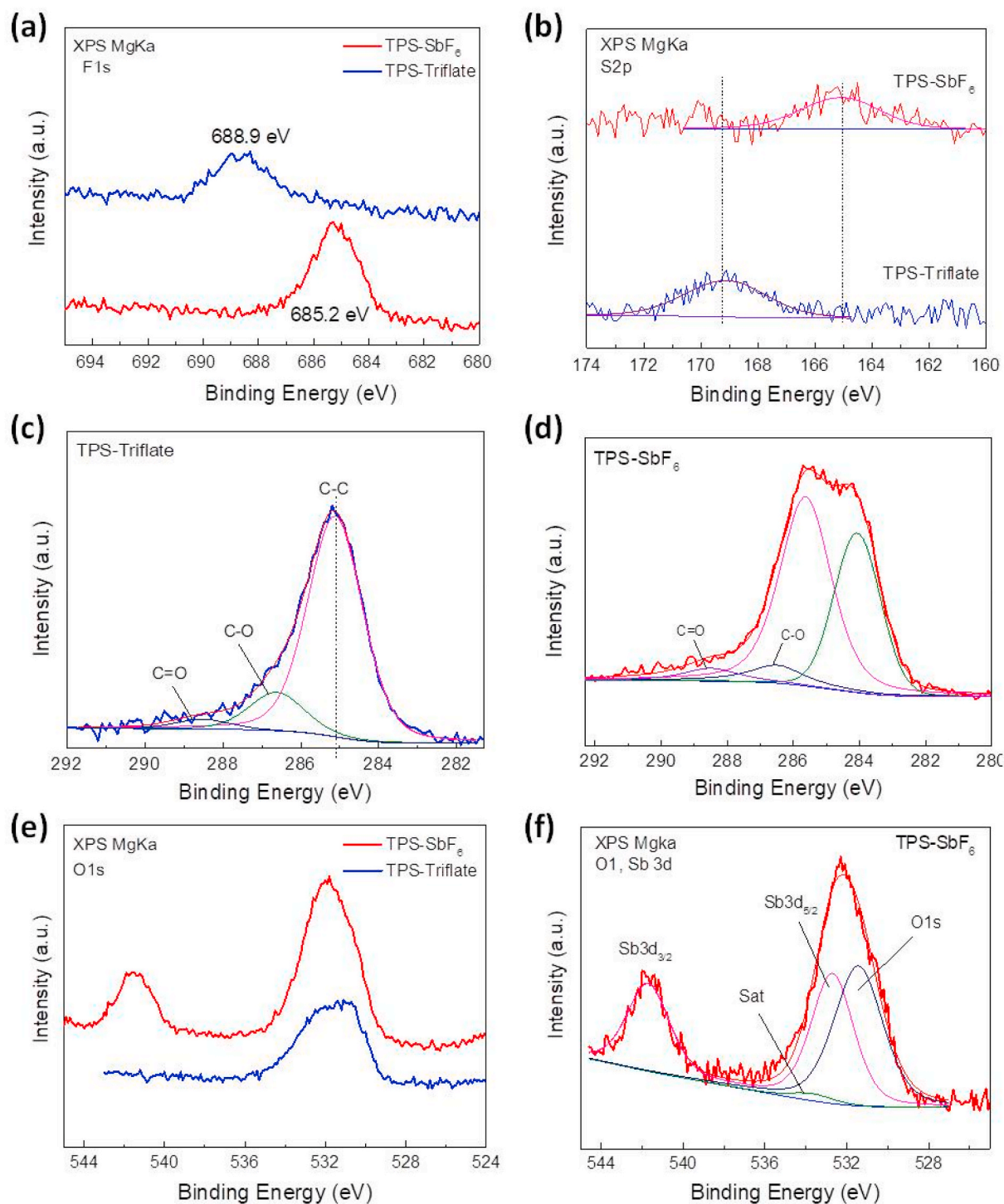


Fig. 2. X-ray photoelectron spectroscopy (XPS) spectra of the (a) F 1s and (b) S 2p peak of TPS-SbF₆ and TPS-Triflate films deposited on ITO. XPS C 1s peaks of (c) TPS-Triflate and (d) TPS-SbF₆. (e) XPS O 1s peaks of TPS-SbF₆ and TPS-Triflate and (f) XPS O 1s and Sb 3d of the TPS-SbF₆ spin-coated on ITO substrates.

salts, we investigate the influence of doping the PEDOT:PSS HIL with two different TPS salts on the OLED performance. These TPS salts consist of different counter anions namely hexafluoroantimonate (termed hereafter as TPS-SbF₆) and trifluoromethane sulfonate (termed as TPS-Triflate). They were added in the PEDOT:PSS solution and employed as HILs in a poly[(9,9-dioctylfluorenyl-2,7-diyl)-co-(1,4-benzo-{2,1',3'}-thiadiazole)] (F8BT) based green emissive OLED. It was demonstrated that the type of the counter anion as well as the concentration of the TPS-salt in the PEDOT:PSS play crucial role in the OLED performance. The addition of these TPS-salts in the PEDOT:PSS matrix induces an increase

in the W_F of the composite HIL, thus improving hole injection at the F8BT/anode interface. Furthermore, TPS-Triflate significantly increases the conductivity of the composite HIL while also induces the formation of an interface exciplex that effectively confines excitons at the anode interface, thus preventing their diffusion towards the cathode interface when they can be quenched by aluminum. Consequently, OLEDs using the TPS-Triflate-doped PEDOT:PSS HIL exhibit a 50% improvement in the device luminance and over 12-fold enhancement in the luminous efficiency compared with the reference device with the pristine PEDOT:PSS HIL. They also demonstrated reduced efficiency roll-off and

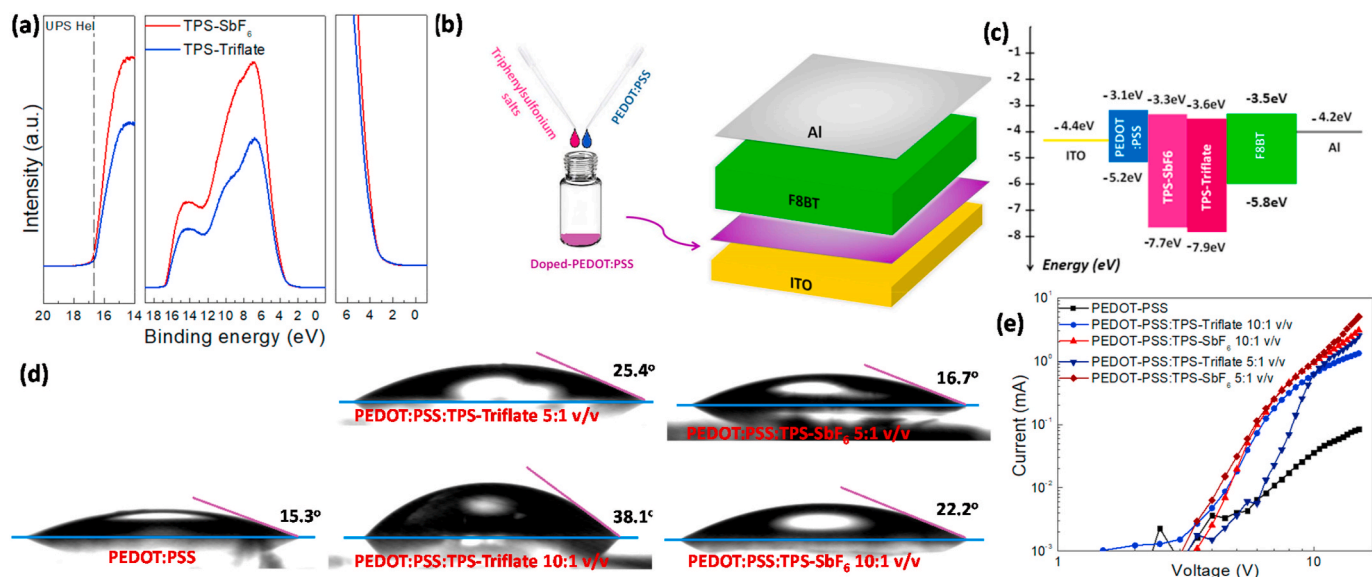


Fig. 3. (a) Ultraviolet photoelectron spectroscopy (UPS) spectra of TPS-SbF₆ and TPS-Triflate deposited on ITO substrates. The whole spectra are presented in the middle, the high BE cut-off and the HOMO region are shown in detail in the left and right parts respectively. (b) Schematic representation of the OLEDs with TPS-salt-doped PEDOT:PSS HIL. (c) Illustration of energy levels of the materials used in the OLED, considering the vacuum level alignment of the OLED layers before physical contact. (d) Water contact angle measurements taken in pristine and TPS-salt doped PEDOT:PSS films. (e) Current versus voltage measured in hole only devices (ITO/HTL/F8BT/MoO_x/Al).

improved lifetime compared to both the reference and the TPS-SbF₆-modified OLEDs.

2. Experimental section

Device Preparation. Coated glass substrates of ITO with sheet resistance 20 Ω/square were used for OLED devices fabrication. The substrates were cleaned in acetone, 2-propanol, and deionized water for 10 min under sonication subsequently and dried with N₂ gas after each bath respectively. PEDOT:PSS solution supplied from Sigma Aldrich was filtered using 0.45 μm PVDF filters. Afterwards, the following organic sulfonium salts, TPS-Triflate and TPS-SbF₆, supplied from Midori Kagaku Co., were dissolved in methanol at a concentration of 10 mg mL⁻¹ and stirred for 2h without heating. Then, the PEDOT:PSS and TPS salts solutions were mixed in various concentrations (0 v/v, 1:10 v/v and 1:5 v/v) and vigorously stirred for 1 h. Note that, concentration of 0 v/v corresponds to the reference sample. Next, the solutions were spin coated on the substrates in ambient conditions to form approximately a 40 nm thin layer (spinning for 40 s at 6000 rpm) and annealed on a hotplate at 100 °C for 1h. Note that the thickness of the prepared HIL films was estimated using a profilometer. The emissive layer was the green-yellow copolymer F8BT, supplied from American Dyes Source. It was processed by a 10 mg mL⁻¹ solution in chloroform. Firstly filtered through a 0.22 μm pore size PTFE filter, it was then spin coated (at 1200 rpm for 40 s to form an 80 nm thin layer) atop HIL in ambient conditions. After deposition, the F8BT film was annealed at 95 °C for 10 min on a hotplate. The devices were completed with a 150 nm aluminum, which served as the cathode electrode, deposited through a shadow mask in a dedicated chamber.

Characterization techniques. Absorption spectra measurements were extracted using a PerkinElmer Lambda 40 UV/Vis spectrophotometer. X-ray photoelectron spectra (XPS) and ultraviolet photoelectron spectra (UPS) were recorded by a Leybold EA-11 electron analyzer. The contact potential difference (CPD) was determined with a single-point Kelvin Probe system (KP010). Photoluminescence spectra in steady-state were extracted by means of a PerkinElmer LS-50B fluorescence spectrometer upon excitation at 380 nm. Normalization of the PL spectra was obtained at the main peak of 540 nm. Field emission

scanning electron microscopy (FE-SEM) measurements were performed on the JEOL JSM-7610FPlus that integrates a full set of detectors for secondary electrons, backscattered electrons, energy dispersive X-ray spectroscopy (EDS). The samples were visualized without any sputtering process. The surface morphology of composite HILs and F8BT films deposited on top of them was recorded with an NT-MDT AFM system in tapping operation mode. Current density-voltage characteristics were measured using a Keithley 2400 source-measure unit. Luminance and electroluminescence spectra were recorded with an Ocean Optics USB 2000 fiber optic spectrophotometer, assuming a Lambertian emission profile (for luminance measurements). All measurements were performed in air at room temperature. Note that all the electroluminescence spectra were measured at 15 V and normalized according to the main peak at 530 nm.

3. Results and discussion

The chemical structure of the materials used as the emissive and HILs in this work, including the copolymer F8BT, the p-type semiconductor PEDOT:PSS, and the two sulfonium salts (TPS-SbF₆ and TPS-Triflate) acting as dopants of PEDOT:PSS are presented in Fig. 1. The TPS-salts are composed of the same TPS cation and two different counter anions hexafluoroantimonate and trifluoromethane sulfonate with main differences in the size of the anion, the organic part content, the presence of Sb, and the number of fluorine (F) atoms therein. In order to evaluate the optoelectronic properties of TPS-salt films, X-ray photoelectron spectroscopy (XPS) was performed. Fig. 2a depicts the F 1s peak of the XPS spectra taken on TPS-SbF₆ and TPS-Triflate films coated on ITO substrates. For the TPS-SbF₆ sample, the F 1s peak is located at 685.2 eV attributed to the F-Sb bond [41], while in the case of TPS-Triflate the peak is shifted in higher binding energy located at 688.9 eV ascribed to the F-C bond. In Fig. 2b, the XPS spectra of S 2p are presented for both TPS-salts. It is observed that the S 2p peak is located in different binding energies, where a peak at 165 eV is appeared in the spectrum of TPS-SbF₆ and another peak at 169.2 eV is present in the TPS-Triflate sample, originated by the S-C bonding and SO₃, respectively, due to the different ionic nature of S cation. Moreover, the XPS spectra of C 1s for TPS-Triflate and TPS-SbF₆ samples are presented in Fig. 2c and d,

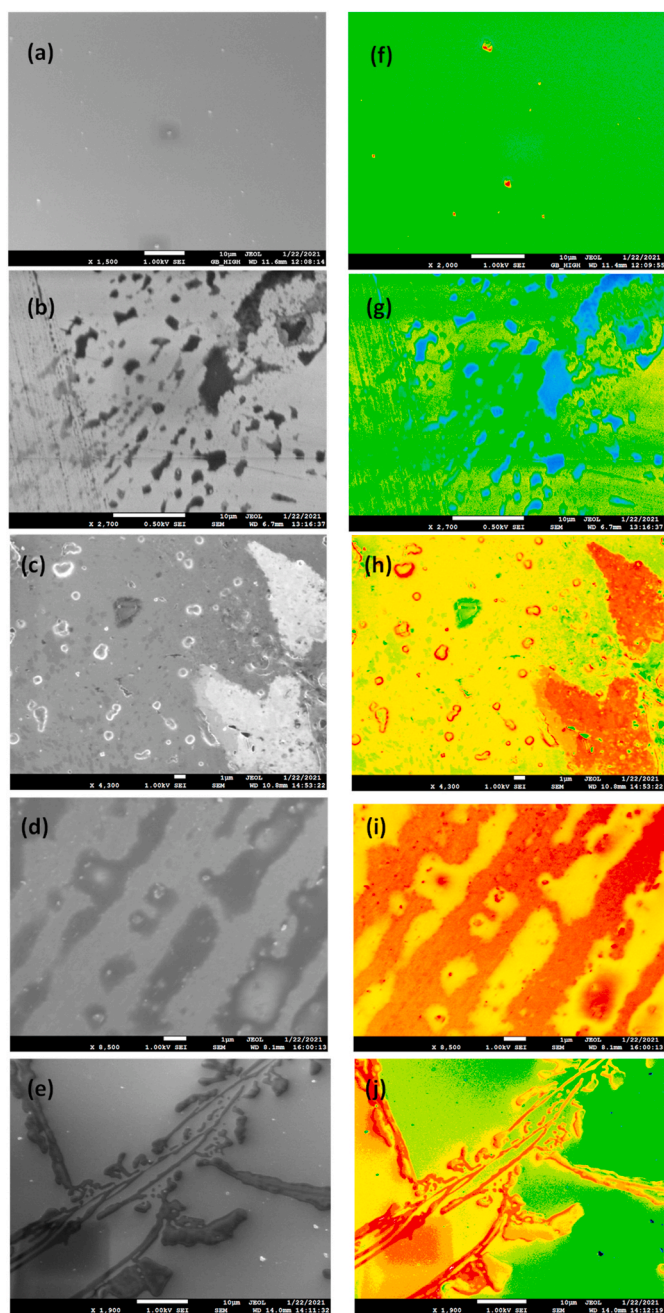


Fig. 4. SEM topographic images of (a,f) PEDOT:PSS, (b,g) PEDOT:PSS:TPS-Triflate 10:1 v/v, (c,h) PEDOT:PSS:TPS-Triflate 5:1 v/v, (d,i) PEDOT:PSS:TPS-SbF₆ 10:1 v/v, and (e,j) PEDOT:PSS:TPS-SbF₆ 5:1 v/v.

respectively. The main C 1s peak of TPS-Triflate is located at 285.1 eV attributed to the C–C bonds, while the other two peaks appeared in the spectrum correspond to the C–O bonds. The contribution of C–C and C–O bonds is also observed in the XPS spectrum of TPS-SbF₆. Furthermore, the XPS spectra of O 1s for both TPS-salts are presented in Fig. 2e. The O 1s spectrum of TPS-SbF₆ is different from that of TPS-Triflate due to the overlap of the Sb 3d and O 1s peaks. Therefore, the spectrum of TPS-SbF₆ is further analyzed, as shown in Fig. 2f. The peak Sb 3d is a doublet, where the Sb 3d_{5/2} is located at 532.7 eV and the Sb 3d_{3/2} at 9 eV higher binding energy (BE). Consequently, the O 1s peak, which is probably associated to the ITO substrate, as well as, the interaction between oxygen and carbon atoms at the surface of the sample, is located at 531.4 eV with a width of 2.8 eV. Note that the peak refers to the satellite peak of Sb 3d_{3/2} due to MgK $\alpha_{2,3}$ radiation. In the

TPS-Triflate sample, the O 1s peak appeared in the XPS spectrum is derived by the contribution of two constituents located at 530.8 eV and 532.5 eV attributed to oxygen atoms of ITO and O–S bonds, respectively.

In addition, the electronic properties such as W_F and highest occupied molecular orbital (HOMO) of the TPS-salt films on ITO substrate were investigated using ultraviolet photoelectron spectroscopy (UPS). The corresponding high-binding energy cut-off (left), the full UPS spectra (middle), and the near Fermi level region of the UPS spectra (right) are presented in Fig. 3a. The TPS-Triflate and TPS-SbF₆ films possess a typical W_F value of 4.6 ± 0.1 eV and 4.5 ± 0.1 eV, respectively, while from the UPS onset (3.3 ± 0.1 eV for the TPS-Triflate and 3.2 ± 0.1 eV for the TPS-SbF₆) their HOMO levels were estimated about 7.9 ± 0.2 and 7.7 ± 0.2 eV, respectively. Such a deep HOMO level of these materials could be beneficial for hole injection as it could induce an upward shift of the vacuum level during the device fabrication thus creating a large positive interfacial dipole (i.e., with its positive pole showing towards the anode) [42], that facilitates hole injection.

However, we used those TPS salts as HILs not in their pristine form, as they couldn't form compact, smooth and pinhole-free films, but as dopants in PEDOT:PSS to form composite HILs for OLEDs with the conventional architecture illustrated in Fig. 3b. The energy level diagram of the materials used in the OLED structure is shown in Fig. 3c (assuming vacuum level alignment before contact). The W_F values of ITO anode and Al cathode, as well as, the HOMO and LUMO levels of F8BT and PEDOT:PSS were taken from our previous work [43]. It is observed that the HOMO levels of both salts are quite deep. The high HOMO levels of TPS-salts are indicative of the formation of a large local electric field at the anode/F8BT interface that reduces the hole injection barrier. However, the LUMO of TPS-Triflate is lower than that of F8BT. A high lying LUMO of the hole injection/transport materials is desired as it ensures efficient electron blocking at the anode interface. We also investigated the properties of the composite material by measurements of the contact potential difference (CPD) of pristine and TPS-salt doped PEDOT:PSS samples using the Kelvin probe technique (Fig. S1, Supporting Information). A pronounced increase in the CPD of PEDOT:PSS was observed upon TPS-salt doping. The influence of the TPS-salts concentration in the PEDOT:PSS solution on the electronic properties of the modified films was also studied. In particular, a significant increase of 0.64 V in the CPD of PEDOT:PSS:TPS-Triflate with concentration of 10:1 v/v with respect to pristine PEDOT:PSS was observed while the CPD difference was further increased for higher TPS-Triflate concentration (CPD of +0.87 V for the PEDOT:PSS:TPS-Triflate with concentration 5:1 v/v). Moreover, a similar but not so pronounced trend in the CPD measurements for the pristine and TPS-SbF₆ doped PEDOT:PSS was observed. The higher CPD of PEDOT:PSS was also increased upon the TPS-SbF₆ doping. The higher CPD of TPS-salt-doped PEDOT:PSS samples is indicative of higher surface W_F of the composite layers compared to pristine PEDOT:PSS. In addition, the intrinsic hydrophilicity of pristine PEDOT:PSS was significantly reduced as shown in Fig. 3d. Through the addition of the TSP-salts the water contact angle was significantly increased (especially upon the addition of TPS-Triflate) which indicates that the composite film became less hydrophilic, a property that might have beneficial effect on the OLED performance and stability. Notably, the TPS-salts are highly transparent (Fig. S2) and had no obvious interference with the absorption (Fig. S3) and photoluminescence (Fig. S4) of F8BT films deposited on the composite HILs.

To confirm the beneficial role of the TPS-salt-doped PEDOT:PSS on the improvement of hole injection, hole only devices (HODs) with the structure ITO/undoped and/or TPS-salt-doped PEDOT:PSS/F8BT/molybdenum oxide/Al were prepared. Note that the MoO_x/Al was introduced to the device in order to block electron transport from the cathode to the emissive layer. The current-voltage (I–V) characteristic curves of the fabricated HODs in a semi-logarithmic scale are shown in Fig. 3e. Obviously, a significant increase in the hole current density is observed for the devices with PEDOT:PSS:TPS-Triflate and PEDOT:PSS:TPS-SbF₆ HILs (irrespective to the concentration of doping), which can be

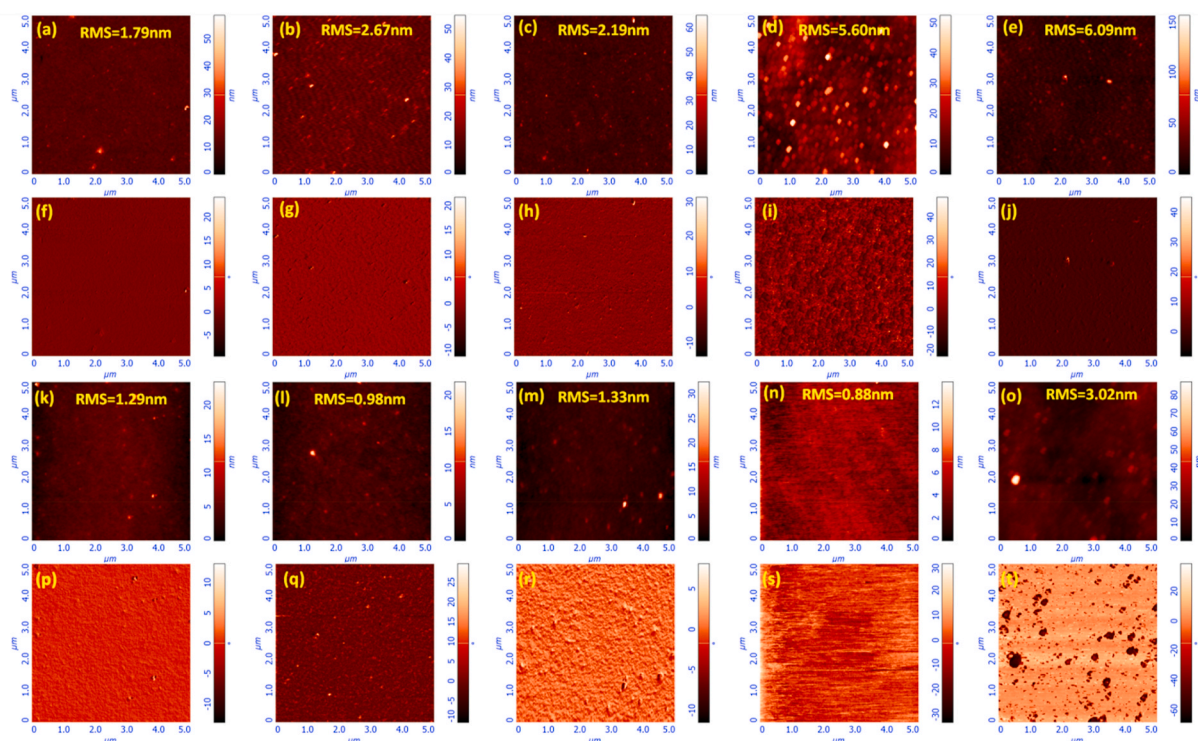


Fig. 5. $5 \times 5 \mu\text{m}^2$ AFM height (a–e) and phase (f–j) images of (a,f) PEDOT:PSS, (b,g) PEDOT:PSS:TPS-Triflate 10:1 v/v, (c,h) PEDOT:PSS:TPS-Triflate 5:1 v/v, (d,i) PEDOT:PSS:TPS-SbF₆ 10:1 v/v, and (e,j) PEDOT:PSS:TPS-SbF₆ 5:1 v/v. $5 \times 5 \mu\text{m}^2$ AFM height (k–o) and phase (p–t) images of F8BT deposited on the pristine and composite HILs presented in (a–e), respectively.

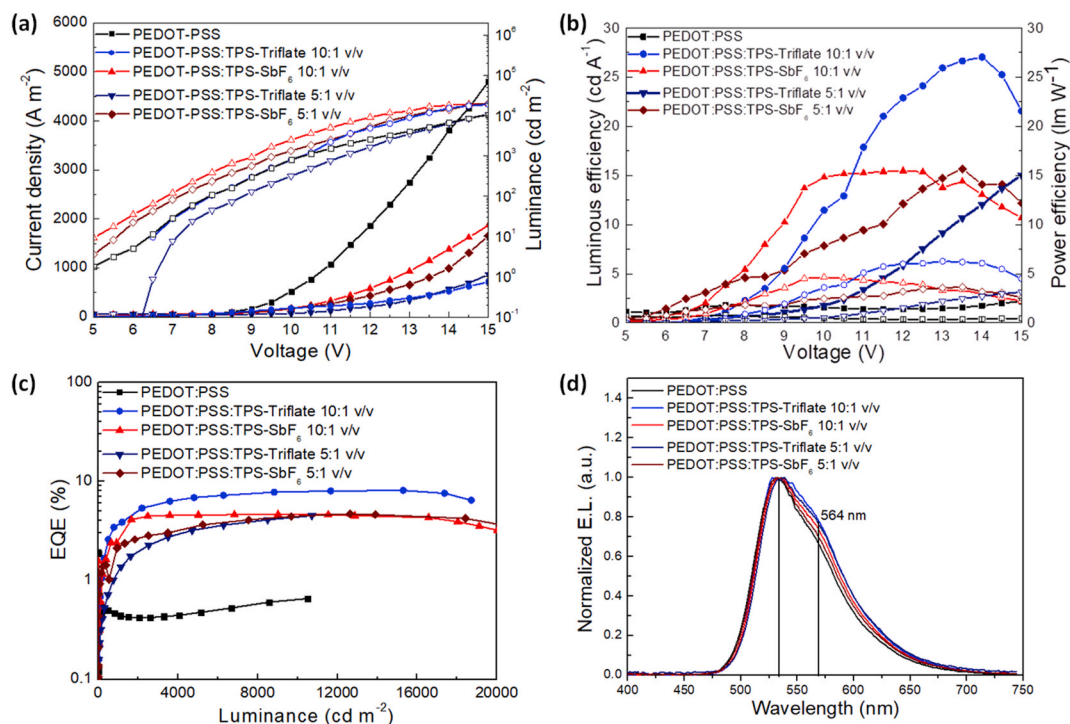


Fig. 6. (a) Current density-luminance-voltage (J-V-L) characteristics (J-V at linear scale and L-V at semilog-scale), (b) luminous efficiency-power efficiency-voltage (LE-PE-V) characteristic curves (in linear scale), (c) EQE-luminance characteristics (in semilog-scale) and (d) electroluminescent (EL) spectra of OLEDs based on F8BT emissive layer with pristine and TPS-salt-doped PEDOT:PSS HILs.

attributed to the improved hole injection due to the increased W_F of the composite films and the reduced hole injection barrier.

Moreover, the addition of TPS-salts in the PEDOT:PSS had a clear

effect on the morphology of the composite films, as revealed by the scanning electron microscopy (SEM) measurements. Fig. 4a and f show the topographic images of the PEDOT:PSS films demonstrating a

Table 1
Performance characteristics of OLEDs based on pristine and TPS-salts-doped PEDOT:PSS HIL as derived from J-V-L curves presented in Fig. 6.

HIL	J_{\max} (A m^{-2})	L_{\max} (Cd m^{-2})	$V_{\text{turn-on}}$ (V) [at 10 Cd m^{-2}]	$V_{\text{operation}}$ (V) [at 1000 Cd m^{-2}]	$L.E._{\max}$ (Cd A^{-1}) [at V]	$P.E._{\max}$ (lm W^{-1}) [at V]
PEDOT:PSS	4804.31	10,492.24	6.42	10.34	2.18 [15.0]	0.75 [7.5]
PEDOT:PSS:TPS-Triflate 10:1 v/v	868.85	18,716.78	6.47	10.25	27.04 [14.0]	6.26 [13.0]
PEDOT:PSS:TPS-SbF ₆ 10:1 v/v	1871.05	20,022.21	5.07	9.14	15.47 [12.0]	4.64 [10.0]
PEDOT:PSS:TPS-Triflate 5:1 v/v	712.91	10,713.72	7.04	11.28	15.02 [15.0]	3.14 [15.0]
PEDOT:PSS:TPS-SbF ₆ 5:1 v/v	1657.55	20,179.97	5.58	9.5	15.67 [13.5]	3.64 [13.5]

homogeneous surface. On the other hand, the formation of aggregates on the TPS-salt doped PEDOT:PSS films is clear evident, which is more pronounced upon the increase in TPS-salt doping (Fig. 4b,g and c,h for PEDOT:PSS:TPS-Triflate with concentration of 10:1 v/v and 5:1 v/v, respectively, and Fig. 4d,i and e,j for the PEDOT:PSS:TPS-SbF₆ samples with concentration of 10:1 v/v and 5:1 v/v, respectively). The nanomorphology of the different HILs, as well as, the surface morphology of

the emissive layer deposited on top of them was further investigated using atomic force microscopy (AFM) measurements. Fig. 5a–e and f–j show the $5 \times 5 \mu m^2$ AFM height and phase images, respectively, of pristine and TPS-salt doped PEDOT:PSS. Rougher surfaces compared with the pristine PEDOT:PSS was observed for the PEDOT:PSS:TPS-SbF₆ films with larger root mean square (RMS) surface roughness (RMS of 1.79 nm for the PEDOT:PSS sample, and 5.60 nm and 6.09 nm for the TPS-SbF₆ doped PEDOT:PSS with concentration of 10:1 v/v and 5:1 v/v, respectively). It is also seen that small particles are dispersed within the composite layer which indicate that TPS-SbF₆ forms aggregates and does not uniformly incorporates into the PEDOT:PSS matrix. For the TPS-Triflate doped PEDOT:PSS samples with concentration of 10:1 v/v and 5:1 v/v, the RMS values were 2.67 nm and 2.19 nm, respectively, revealing smoother surfaces compared with the composite films based on TPS-SbF₆ which may improve the F8BT film formation atop, as well. However, no significant effect on the morphology of F8BT films coated on top of TPS-doped-PEDOT:PSS was observed, as shown in Fig. 5k–o (Fig. 5p–t is referred to the $5 \times 5 \mu m^2$ AFM phase images of the same samples). The slight RMS reduction of the F8BT deposited on the composite HILs may improve interfacial contact between the anode and the emissive copolymer. Furthermore, the addition of TPS-Triflate in PEDOT:PSS (1:5 v/v) increased the conductivity of a PEDOT:PSS for nearly one order of magnitude; only a small conductivity enhancement was obtained upon the addition of TPS-SbF₆ in PEDOT:PSS.

The effect of counter anion as well as the concentration of TPS salts in the PEDOT:PSS HIL on the device performance was then investigated. Fig. 6a presents the current density–luminance–voltage (J–L–V) (J–V at linear scale and L–V at semilog-scale) characteristic curves of the fabricated OLEDs. The devices operational characteristics are also summarized in Table 1. It is observed that all devices based on TPS-salt modified PEDOT:PSS HIL exhibit a large decrease in current density and higher luminance values with respect to the reference device using the unmodified PEDOT:PSS as HIL. The highest luminance values were obtained for the OLEDs with the PEDOT:PSS:TPS-SbF₆ (20,179.97 cd m^{-2} and 20,022.21 cd m^{-2} for the TPS-SbF₆ modified PEDOT:PSS with concentration 5:1 v/v and 10:1 v/v, respectively). The device using the

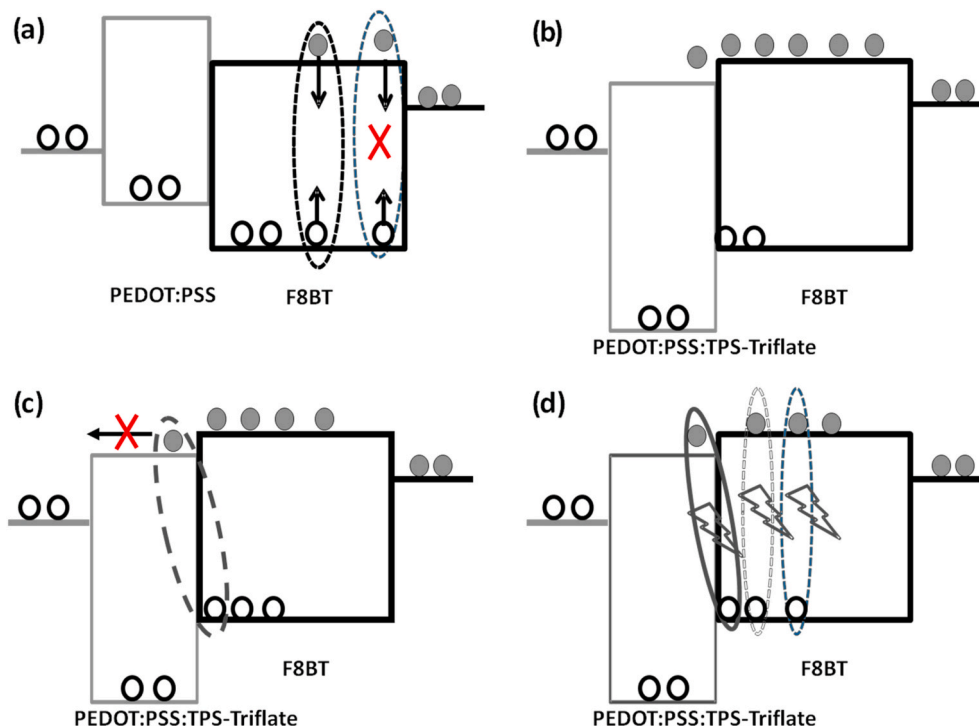


Fig. 7. Proposed EL mechanisms in the OLEDs with (a) pristine PEDOT:PSS and (b–d) composite PEDOT:PSS:TPS-salt HIL. The interface exciplex formation and its emission at longer wavelengths are also illustrated.

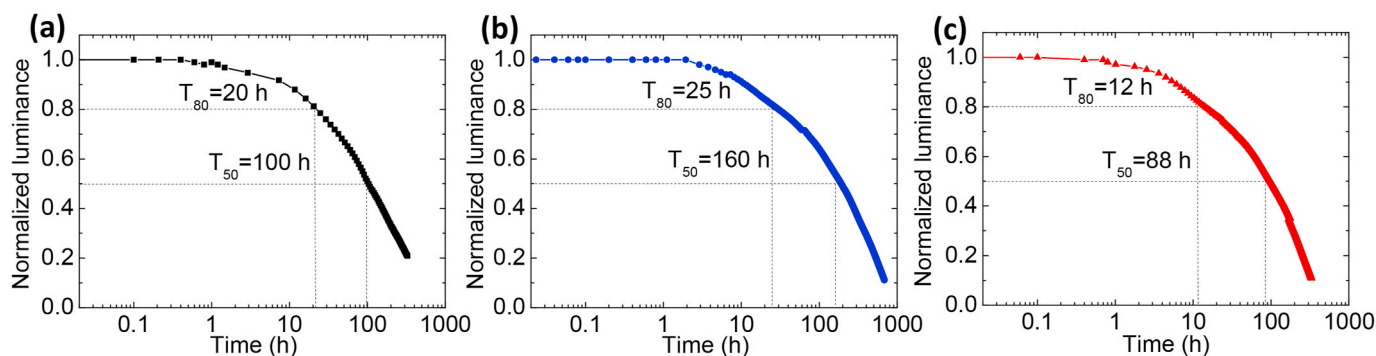


Fig. 8. Plot of normalized luminance versus time for continuously operating OLEDs at an initial luminance of 1000 cd m^{-2} using (a) PEDOT:PSS, (b) PEDOT:PSS:TPS-Triflate 10:1 v/v, and (c) PEDOT:PSS:TPS-SbF₆ 10:1 v/v hole injection layers. The estimated lifetimes are also shown.

PEDOT:PSS:TPS-Triflate 5:1 v/v as HIL exhibited a high L value of $18,716.78 \text{ cd m}^{-2}$, while the OLED with the PEDOT:PSS:TPS-Triflate 10:1 v/v showed a luminance of $10,713.72 \text{ cd m}^{-2}$, which was comparable with that of the reference device ($10,492.24 \text{ cd m}^{-2}$). Moreover, reduced turn-on voltage ($V_{\text{turn-on}}$) values were observed for both devices based on TPS-SbF₆ modified PEDOT:PSS, while in the case of PEDOT:PSS:TPS-Triflate OLEDs the $V_{\text{turn-on}}$ was nearly similar to the reference one. The significant drop in $V_{\text{turn-on}}$ of the TPS-SbF₆ including devices can be attributed to a lower hole injection barrier as its HOMO level is closer to that of F8BT compared to TPS-Triflate. The luminous (LE) and power (PE) efficiencies, however, were significantly increased upon PEDOT:PSS modification with TPS-salts, as presented in Fig. 6b (in linear scale) and Table 1. In particular, PEDOT:PSS:TPS-Triflate with the concentration of 10:1 v/v represents an increase by a factor of more than 12 for the LE and 8 for the PE with respect to the reference device. The latter can be explained on the basis of more balanced carrier transport within the device using the composite HIL, especially in the case of TPS-Triflate doped PEDOT:PSS. However, the extraordinary charge balance in the TPS-Triflate embedding device cannot be explained if we take into account the reduced electron blocking capability of this material (since its LUMO level is lower than that of F8BT). On the other hand, the PEDOT:PSS:TPS-SbF₆ based OLEDs presents lower LE and PE values compared to that using the TPS-Triflate doped PEDOT:PSS, even though it exhibits enhanced electron blocking ability (its LUMO lies above that of F8BT). Furthermore, Fig. 6c shows the external quantum efficiency (EQE) versus luminance characteristic curves of the prepared OLEDs (in a semi-log scale). It is observed that high and stable EQEs are achieved for all devices based on the TPS-salt doped PEDOT:PSS hole injection layer. Especially, the maximum efficiency of 8.1% at $11,000 \text{ cd m}^{-2}$ was reported for the device using the PEDOT:PSS:TPS-Triflate with the concentration of 10:1 v/v HIL, representing an enormous EQE improvement compared with the efficiency of the reference device (0.66% at $10,500 \text{ cd m}^{-2}$). It is noteworthy that our champion device also exhibited a low efficiency roll-off: achieved EQE of 7.6% at $17,000 \text{ cd m}^{-2}$, corresponding to 6.17% efficiency's decrease at the pointed luminance values.

Moreover, the normalized electroluminescence (EL) spectra of the OLEDs based on the unmodified and TPS-salts modified PEDOT:PSS are shown in Fig. 6d. The EL peak at 530 nm corresponds to the HOMO-LUMO difference of F8BT. However, a small broadening towards higher wavelengths in the EL spectra of the TPS-salt-modified PEDOT:PSS OLEDs is observed. This broadening is not seen in the normalized PL spectra of F8BT films deposited on TPS-Triflate modified PEDOT:PSS, Figs. S5 and S6. This broadening is due to the appearance of a second peak at the EL spectrum at around 564 nm, which corresponds to the energy difference between the F8BT's HOMO and TPS-Triflate's LUMO (2.2 eV) and is indicative of the formation of an interface exciplex that is an excited state complex between the TPS-Triflate (acting as the donor constituent of the excited state complex) and F8BT (that acts as the

acceptor in the exciplex. Exciplex formation under electrical excitation is easier to be identified as the molecular local excited states are more pronounced in the donor:acceptor spectrum taken under optical excitation [44]. This, along with the small degree of exciplex formation as it is formed at the TPS-salt/F8BT interface, can explain the lack of exciplex emission in the PL spectrum. The proposed mechanism for interface exciplex formation is as follows: upon forward bias in the PEDOT:PSS based device, hole and electron injection occurs to form excitons within the F8BT. These excitons are uniformly formed within the EML due to the ambipolar charge transport of F8BT. However, excitons formed near the cathode interface are quenched thus reducing the device EL efficiency (Fig. 7a). In the TPS-Triflate embedding device, the lower LUMO level of this salt compared to that of F8BT results in electron leakage towards the HIL (Fig. 7b). These electrons, instead of leaking towards the anode, they form interface exciplexes with holes already present at the HOMO of F8BT (Fig. 7c). The interfacial exciplexes have been recently considered as extremely advantageous for the device performance as they have found to exhibit thermally activated delay fluorescence (TADF) character, thus spatially confining excitons and enhance radiative recombination by preventing excitons from reaching the aluminum contact where they are quenched as illustrated in Fig. 7d [45]. Moreover, they have also shown to reduce the efficiency roll-off and, importantly, to enhance the device lifetime [46–48]. Fig. 8 demonstrates improved lifetime, in particular, T_{80} (attributed to the time where 80% loss of initial luminance is observed) and T_{50} (representing the time corresponding to loss of half of the initial luminance) is obtained for the TPS-Triflate modified device compared to the reference. This observation explains the best performance of the TPS-Triflate salt based OLED which exhibits the stronger interfacial exciplex formation. The small decrease in device lifetime of OLEDs based on TPS-SbF₆ might be related to the large current density exhibited by this device; however, further investigation is needed which is beyond the scope of the present work.

4. Conclusion

This work reports the application of triphenylsulfonium salts as dopants of the commonly used PEDOT:PSS HIL to enhance hole injection/transport as well as radiative recombination through the formation of an interface exciplex. The type of the counter anion (Triflate or SbF₆) and the concentration of the TPS-salt in the PEDOT:PSS HIL play a crucial role in the device performance. TPS-Triflate-doped sample exhibits much higher luminous and power efficiency than the reference devices attributed not only to a lowering in the W_F but also to a significant increase in conductivity of the composite HIL. The enhancement in radiative recombinations can also be explained on the basis of the formation of an interface exciplex between TPS-Triflate and F8BT, which can also explain the reduced efficiency roll-off and the elongated device lifetime. This work demonstrates a simple and efficient solution-

processed strategy to modify the interfacial energy level alignment and hole injection in OLEDs by using appropriately triphenylsulfonium salts, illustrating the feasibility for their implementation in other organic and perovskite optoelectronic devices.

Declaration of competing interest

The authors declare that they have no known competing financial interests or personal relationships that could have appeared to influence the work reported in this paper.

Acknowledgements

The research work has supported by the Hellenic Foundation for Research and Innovation (H.F.R.I.) under the “First Call for H.F.R.I. Research Projects to support Faculty members and Researchers and the procurement of high-cost research equipment grant” (project Number: 356.0001).

Appendix A. Supplementary data

Supplementary data to this article can be found online at <https://doi.org/10.1016/j.orgel.2021.106155>.

References

- [1] C.W. Tang, S.A. Vanslyke, *Appl. Phys. Lett.* 51 (1987) 913–915.
- [2] H. Yan, Q. Huang, B.J. Scott, T.J. Marks, *Appl. Phys. Lett.* 84 (2004) 3873–3875.
- [3] Y. Sun, N.C. Giebink, H. Kanno, B. Ma, M.E. Thompson, S.R. Forrest, *Nature* 440 (2006) 908–912.
- [4] M. Sessolo, H.J. Bolink, *Adv. Mater.* 23 (2011) 1829–1845.
- [5] L.C. Palilis, M. Vasilopoulou, D.G. Georgiadou, P. Argitis, *Org. Electron.* 11 (2010) 887.
- [6] X. Ren, B.D. Alleyne, P.I. Djurovich, C. Adachi, I. Tsyba, R. Bau, M.E. Thompson, *Inorg. Chem.* 43 (2004) 1697–1707.
- [7] X. Gong, D. Moses, A.J. Heeger, S. Liu, A.K.Y. Jen, *Appl. Phys. Lett.* 83 (2003) 183–185.
- [8] R.D. Hreha, C.P. George, A. Haldi, B. Domercq, M. Malagoli, S. Barlow, J.L. Brédas, B. Kippelen, S.R. Marder, *Adv. Funct. Mater.* 13 (2003) 967–973.
- [9] S. Shahnawaz, S. Sudheendran Swayamprabha, M.R. Nagar, R.A.K. Yadav, S. Gull, D.K. Dubey, J.H. Jou, *J. Mater. Chem. C* 7 (2019) 7144–7158.
- [10] S. Negi, P. Mittal, B. Kumar, *Microsyst. Technol.* 24 (2018) 4981–4989.
- [11] H.R. Kim, T.W. Kim, S.G. Park, *Polym. Int.* 68 (2019) 1478–1483.
- [12] M. Baek, J. Shin, D. Hwang, S. Kim, H. Park, S. Park, *Crystals* 10 (8) (2020) 645.
- [13] M. Vasilopoulou, A.M. Douvas, D.G. Georgiadou, L.C. Palilis, S. Kennou, L. Sygellou, A. Soultati, I. Kostis, G. Papadimitropoulos, D. Davazoglou, P. Argitis, *J. Am. Chem. Soc.* 134 (2012) 16178–16187.
- [14] M. Vasilopoulou, G. Papadimitropoulos, L.C. Palilis, D.G. Georgiadou, P. Argitis, S. Kennou, I. Kostis, N. Vourdas, N.A. Stathopoulos, D. Davazoglou, *Org. Electron.* 13 (2012) 796–806.
- [15] W.T. Wu, C.M. Hsu, W.M. Lin, D.H. Tsai, U.J. Peng, *Org. Electron.* 30 (2016) 219–224.
- [16] H. Lee, S. Member, *Jnl Soc Info Display* 20 (2012) 640–645.
- [17] T.L. Chiu, Y.T. Chuang, *J. Nanosci. Nanotechnol.* 15 (2015) 9207–9211.
- [18] Y.H. Li, X. Lu, R. Wang, Y.Y. Ma, S. Duhm, M.K. Fung, *J. Mater. Chem. C* 5 (2017) 11751–11757.
- [19] P. Kumar, N. Agrawal, S.D. Choudhary, A.K. Gautam, *IEEE Trans. Nanotechnol.* 19 (2020) 61–66.
- [20] P.J. Jesuraj, H. Hafeez, S.H. Rhee, D.H. Kim, J.C. Lee, W.H. Lee, D.K. Choi, A. Song, K.B. Chung, M. Song, C.S. Kim, S.Y. Ryu, *Org. Electron.* 56 (2018) 254–259.
- [21] A.M. Douvas, M. Vasilopoulou, D.G. Georgiadou, A. Soultati, D. Davazoglou, N. Vourdas, K.P. Giannakopoulos, A.G. Kontos, S. Kennou, P. Argitis, *J. Mater. Chem. C* 2 (31) (2014) 6290–6300.
- [22] S. Kirchmeyer, K. Reuter, *J. Mater. Chem.* 15 (2005) 2077–2088.
- [23] X. Yang, H. Guo, B. Liu, J. Zhao, G. Zhou, Z. Wu, W.Y. Wong, *Adv. Sci.* 5 (2018) 1800950.
- [24] S.Y. Lee, T. Yasuda, H. Komiyama, J. Lee, C. Adachi, *Adv. Mater.* 28 (2016) 4019–4024.
- [25] Y. Xia, J. Ouyang, *Org. Electron.* 11 (2010) 1129–1135.
- [26] M.A. Guzjak, T. Nishizaki, Y. Honma, K. Watanabe, T. Sasaki, *Trans. Mater. Res. Soc. Japan.* 38 (2013) 363–367.
- [27] Z. Shahedi, M.R. Jafari, *Appl. Phys. Mater. Sci. Process* 123 (2017) 1–9.
- [28] C. Badre, L. Marquant, A.M. Alsayed, L.A. Hough, *Adv. Funct. Mater.* 22 (2012) 2723–2727.
- [29] G.F. Wang, X.M. Tao, R.X. Wang, *Compos. Sci. Technol.* 68 (2008) 2837–2841.
- [30] J. Park, A. Lee, Y. Yim, E. Han, *Synth. Met.* 161 (2011) 523–527.
- [31] N. Kim, S. Kee, S.H. Lee, B.H. Lee, Y.H. Kahng, Y.R. Jo, B.J. Kim, K. Lee, *Adv. Mater.* 26 (2014) 2268–2272.
- [32] R.A.K. Yadav, M.R. Nagar, D.K. Dubey, S.S. Swayamprabha, J.-H. Jou, *MRS Advances* 4 (2019) 1779–1786.
- [33] S.-H. Jeong, H. Kim, M.-H. Park, Y. Lee, N. Li, H.-K. Seo, T.-H. Han, S. Ahn, J.-M. Heo, K.S. Kim, T.-W. Lee, *Nanomater. Energy* 60 (2019) 324–331.
- [34] M. Zeng, X. Wang, R. Ma, W. Zhu, Y. Li, Z. Chen, J. Zhou, W. Li, T. Liu, Z. He, H. Yan, F. Huang, Y. Cao, *Adv. Energy Mater.* 10 (2020) 2000743.
- [35] J.V. Crivello, *Adv. Polym. Sci.* 62 (1984) 1.
- [36] I. Raptis, D. Velessiotis, M. Vasilopoulou, P. Argitis, *Microelectron. Eng.* 53 (1–4) (2000) 489–492.
- [37] E. Reichmanis, F.M. Houlihan, O. Nalamasu, T.X. Neenan, *Chem. Mater.* 3 (1991) 394–407.
- [38] D.G. Georgiadou, L.C. Palilis, M. Vasilopoulou, G. Pistolis, D. Dimotikali, P. Argitis, *J. Mater. Chem.* 21 (2011) 9296–9301.
- [39] D.G. Georgiadou, L.C. Palilis, M. Vasilopoulou, G. Pistolis, D. Dimotikali, P. Argitis, *Synth. Met.* 181 (2013) 37–44.
- [40] M. Vasilopoulou, D. Georgiadou, G. Pistolis, P. Argitis, *Adv. Funct. Mater.* 17 (2007) 3477–3485.
- [41] T. Birchall, J.A. Connor, L.H. Hillier, *J. Chem. Soc., Dalton Trans.* (1975) 2003–2006.
- [42] Q. Chen, C. Wang, Y. Li, L. Chen, *J. Am. Chem. Soc.* 20 (2020) 18281–18292.
- [43] M. Tountas, Y. Topal, M. Kus, M. Ersöz, M. Fakis, P. Argitis, M. Vasilopoulou, *Adv. Funct. Mater.* 26 (2016) 2655–2665.
- [44] N. Bunzmann, S. Weißenseel, L. Kudriashova, J. Grüne, B. Krugmann, J. V. Grazulevicius, A. Sperlich, V. Dyakonov, *Mater. Horiz.* 7 (2020) 1126–1137.
- [45] M. Colella, P. Pander, D.D.S. Pereira, A.P. Monkman, *ACS Appl. Mater. Interfaces* 10 (2018) 40001–40007.
- [46] S.O. Jeon, S.E. Jang, H.S. Son, J.Y. Lee, *Adv. Mater.* 23 (2011) 1436–1441.
- [47] W. Song, H.L. Lee, J.Y. Lee, *J. Mater. Chem.* 5 (2017) 5923–5929.
- [48] P.L. dos Santos, Dias, A.P. Monkman, *J. Phys. Chem. C* 120 (32) (2016) 18259–18267.